2D MATERIALS

PROPERTIES AND DEVICES

EDITED BY PHAEDON AVOURIS, TONY F. HEINZ, AND TONY LOW

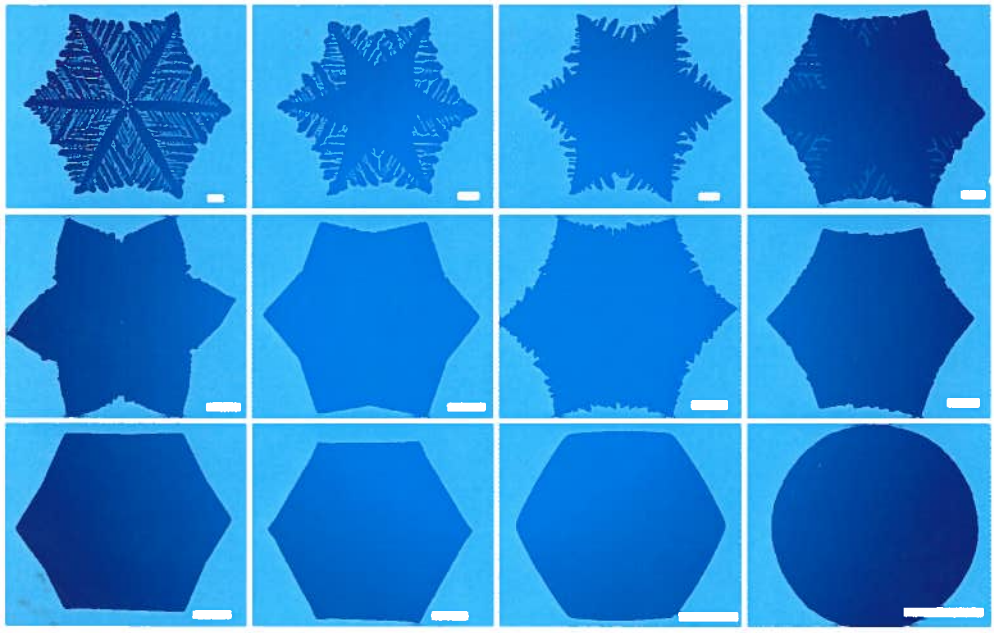

CAMBRIDGE

MRS MATERIALS RESEARCH SOCIETY®
Advancing materials. Improving the quality of life.

CAMBRIDGE
UNIVERSITY PRESS

University Printing House, Cambridge CB2 8BS, United Kingdom

One Liberty Plaza, 20th Floor, New York, NY 10006, USA

477 Williamstown Road, Port Melbourne, VIC 3207, Australia

4843/24, 2nd Floor, Ansari Road, Daryaganj, Delhi – 110002, India

79 Anson Road, #06–04/06, Singapore 079906

Cambridge University Press is part of the University of Cambridge.

It furthers the University's mission by disseminating knowledge in the pursuit of education, learning, and research at the highest international levels of excellence.

www.cambridge.org
Information on this title: www.cambridge.org/9781107163713
10.1017/9781316681619

First published 2017

Printed in the United Kingdom by TJ International Ltd. Padstow Cornwall.

A catalogue record for this publication is available from the British Library.

Library of Congress Cataloging-in-Publication Data
Names: Avouris, Phaedon, 1945- editor. | Heinz, Tony F., editor. | Low, Tony, editor.
Title: 2D materials : properties and devices / edited by Phaedon Avouris (IBM T.J. Watson Research Center, New York), Tony F. Heinz (Stanford University and SLAC National Accelerator Laboratory), Tony Low (University of Minnesota).
Other titles: Two dimensional materials
Description: Cambridge, United Kingdom ; New York, NY : Cambridge University Press, 2017. | Includes bibliographical references and index.
Identifiers: LCCN 2016043383| ISBN 9781107163713 (Hardback ; alk. paper) | ISBN 1107163714 (hardback ; alk. paper)
Subjects: LCSH: Graphene. | Nanostructured materials.
Classification: LCC TA455.G65 A15 2017 | DDC 620.1/15–dc23
LC record available at https://lccn.loc.gov/2016043383

ISBN 978-1-107-16371-3 Hardback

Contents

Contributors

Thierry Angot
Aix-Marseille Université

Phaedon Avouris
IBM T. J. Watson Research Center

Alexander A. Balandin
University of California, Riverside

S. Cahangirov
Bilkent University

Luiz Gustavo Cançado
Federal University of Minas Gerais

Andres Castellanos-Gomez
Instituto Madrileño de Estudios Avanzados en Nanociencia

Andrey Chaves
Universidade Federal do Ceara

Jian-Hao Chen
Peking University

S. Ciraci
Bilkent University

Aron W. Cummings
ICN2 – Catalan Institute of Nanoscience and Nanotechnology (CSIC and the Barcelona Institute of Science and Technology)

Cory.R. Dean
Columbia University

[24] S. Kumar and D. M. Parks, "A comprehensive lattice-stability limit surface for graphene," cond-mat.mtrl-sci arXiv:1503.03944v2, March 16, 2014.
[25] Y. Baskin and L. Meyer, "Lattice constants of graphite at low temperatures," *Physical Review*, vol. 100, 544, 1955.
[26] R. C. Cooper, C. Lee, C. A. Marianetti, X. Wei, J. Hone, and J. W. Kysar, "Nonlinear elastic behavior of two-dimensional molybdenum disulfide," *Physical Review B – Condensed Matter and Materials Physics*, vol. 87, 035423, 2013.
[27] R. C. Cooper, J. W. Kysar, and C. A. Marianetti, "Comment on 'ideal strength and phonon instability in single-layer MoS2'," *Physical Review B – Condensed Matter and Materials Physics*, vol. 90, pp. 1–3, 2014.
[28] E. Cadelano, P. L. Palla, S. Giordano, and L. Colombo, "Nonlinear elasticity of monolayer graphene," *Physical Review Letters*, vol. 102, pp. 1–4, 2009.
[29] F. Liu, P. Ming, and J. Li, "Ab initio calculation of ideal strength and phonon instability of graphene under tension," *Physical Review B – Condensed Matter and Materials Physics*, vol. 76, pp. 1–7, 2007.
[30] X. Wei and J. W. Kysar, "Experimental validation of multiscale modeling of indentation of suspended circular graphene membranes," *International Journal of Solids and Structures*, vol. 49, pp. 3201–9, 2012.
[31] Y. F. Gao and A. F. Bower, "A simple technique for avoiding convergence problems in finite element simulations of crack nucleation and growth on cohesive interfaces," *Modelling and Simulation in Materials Science and Engineering*, vol. 12, pp. 453–63, 2004.
[32] S. Kumar and D. M. Parks, "On the hyperelastic softening and elastic instabilities in graphene," *Proceedings of the Royal Society of London A: Mathematical, Physical and Engineering Sciences*, vol. 471, 2014.
[33] C. A. Marianetti and H. G. Yevick, "Failure mechanisms of graphene under tension," *Physical Review Letters*, vol. 105, pp. 1–4, 2010.
[34] T. K. Caughey and R. T. Shield, "Instability and the energy criterion for continuous systems," *Journal of Applied Mathematics and Physics* vol. 19, pp. 485–92, 1968.
[35] S. P. Koenig, L. Wang, J. Pellegrino, and J. S. Bunch, "Selective molecular sieving through porous graphene," *Nature Nanotechnology*, vol. 7, pp. 728–32, 2012.
[36] L. G. Cançado, A. Jorio, E. H. M. Ferreira, *et al.*, "Quantifying defects in graphene via Raman spectroscopy at different excitation energies," *Nano Letters*, vol. 11, pp. 3190–6, 2011.
[37] D. C. Kim, D.-Y. Jeon, H.-J. Chung, Y. Woo, J. K. Shin, and S. Seo, "The structural and electrical evolution of graphene by oxygen plasma-induced disorder," *Nanotechnology*, vol. 20, 375703, 2009.
[38] M. M. Lucchese, F. Stavale, E. H. M. Ferreira, *et al.*, "Quantifying ion-induced defects and Raman relaxation length in graphene," *Carbon*, vol. 48, pp. 1592–7, 2010.
[39] A. Eckmann, A. Felten, A. Mishchenko, *et al.*, "Probing the nature of defects in graphene by Raman spectroscopy," *Nano Letters*, vol. 12, pp. 3925–30, 2012.
[40] P. T. Araujo, M. Terrones, and M. S. Dresselhaus, "Defects and impurities in graphene-like materials," *Materials Today*, vol. 15, pp. 98–109, 2012.
[41] A. Zandiatashbar, G. H. Lee, S. J. An, *et al.*, "Effect of defects on the intrinsic strength and stiffness of graphene," *Nature Communications*, vol. 5, p. 3186, 2014.
[42] R. Grantab, V. B. Shenoy, and R. S. Ruoff, "Anomalous strength characteristics of tilt grain boundaries in graphene," *Science*, vol. 1456, pp. 10–13, 2010.
[43] Q. Lu and R. Huang, "Nonlinear mechanics of single-atomic-layer graphene sheets," *International Journal of Applied Mechanics*, vol. 01, pp. 443–67, 2009.

5 Vibrations in Graphene

Ado Jorio, Luiz Gustavo Cançado, and Leandro M. Malard

5.1 Structure and Vibrations of Monolayer Graphene

The organization of atoms in a crystalline structure imposes symmetry-related constrains on the net motion, which influences most properties of solid state systems. In the group theory framework [1], the hexagonal symmetry of monolayer graphene on isotropic medium belongs to the space group P6/*mmm* (D_{6h}^{1}), with two inequivalent C atoms in the unit cell [1, 2, 3, 4]. The unit cell is illustrated in the left sketch of Fig. 5.1(a), defined by the vectors $\vec{a_1}$ and $\vec{a_2}$. Strain can break the hexagonal symmetry, as indicated by the other sketches in Figs. 5.1(a) and (b), with implications on the vibrational structure.

5.1.1 Graphene in an Isotropic Medium

The graphene phonon dispersion is plotted in Fig. 5.2(a). The two unit-cell atoms moving in the three-dimensional space generate six phonon branches – three acoustic (A), with in-phase displacements of the two unit-cell atoms, and three optical (O), with out-of-phase displacements of the two unit-cell atoms. The phonon eigenvectors are described by the acoustic and optical unit-cell displacements multiplied by a wavevector q, which defines the phase modulation along the unit cells in the crystalline lattice. Figure 5.2(a) shows the phonon frequencies with q along the Γ–K direction in the hexagonal Brillouin zone. Figure 5.2(b) shows the 12 phonon eigenvectors at the Γ and K points. The atomic displacements in the graphene plane (i for in-plane) can be longitudinal (L) or transversal (T) with respect to the phonon wavevector direction. The atomic displacements perpendicular to the graphene plane (o for out-of-plane) are transversal (T) phonons, and they generally exhibit lower frequencies because the out-of-plane restoring forces are much weaker than the in-plane ones.

At the Γ point ($q = 0$), the group of wavevector is isomorphic to the point group D_{6h}, which has the special property of being homogeneous for in-plane lattice distortions [1, 2, 4]. Consequently, the in-plane longitudinal optical (iLO) and the in-plane transversal optical (iTO) phonons are degenerate, representing the only first-order Raman active mode of graphene, named G band, belonging to the double-degenerate irreducible representation E_{2g}, appearing at 1584 cm^{-1} [4, 5, 6, 7]. The relatively high frequency of this optical phonon (~0.2 eV) allows the use of Raman spectroscopy to probe small environmental perturbations, including variations in strain [8], doping [9], and

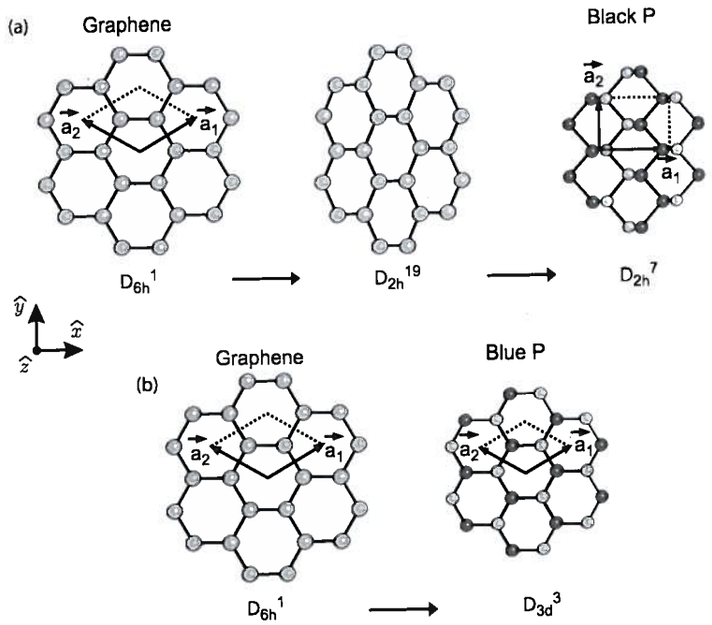

Fig. 5.1 Atomic structure of graphene and the effect of lattice distortion [3]. (a) Starting from graphene (left) and inducing a compressive strain along the $\hat{x}$ direction leads to a phase transition to the space group D_{2h}^{19} (middle), and subsequently to the space group D_{2h}^7 (right), where light and dark gray atoms are at different levels along the $\hat{z}$ direction, which is the structure of black phosphorene. (b) Starting from graphene (left), a bi-axial compressive homogeneous strain leads to a phase transition to D_{3d}^3 space group (right), again with light and dark gray atoms at different levels along the $\hat{z}$ direction, which is the structure of blue phosphorene.

temperature [10]. The out-of-plane transversal optical mode (oTO) at the Γ point is active in infrared absorption spectroscopy [2]. However, the polar character of this vibrational mode is very weak because graphene is homoatomic, and infrared spectroscopy is mostly used to measure the vibrations from functionalization agents and other contaminants in graphene [11, 12], besides direct electronic effects near the K point [13, 14].

The lines in the graphene phonon dispersion plot in Fig. 5.2(a) are theoretical calculations [15], and the symbols are experimental data from inelastic light-scattering [16]. Force constant models are generally used for describing phonon dispersion in materials, but they rely on a limited number of atomic neighbor interactions and do not account for electron–vibration interactions [6]. Graphene, however, has long-range and non-adiabatic effects that had to be considered before an accurate description of the phonon dispersion could be achieved [15, 17, 18, 19, 20, 21].

Experimentally, due to momentum conservation requirements, most materials rely on either neutron or X-ray inelastic scattering to probe phonon dispersion [22, 23], necessary for achieving scattering by phonons in the interior of the Brillouin zone. Graphene, however, has a combination of factors that generate unique effects making it possible to probe the phonon dispersion with inelastic light-scattering in the visible

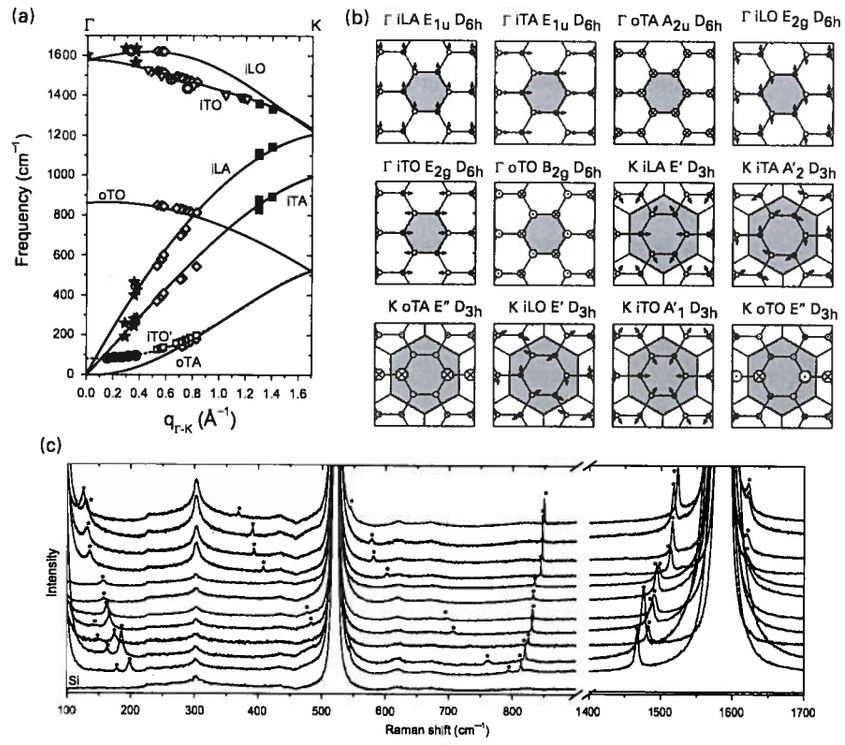

Fig. 5.2 (a) Phonon dispersion of graphene [1, 16]. The solid lines stand for the phonon frequencies (branch assignment near each curve) as a function of wavevector q in the Γ–K direction, taken from [15]. ◊ and □ symbols correspond to the frequencies of the peaks marked by * in the Raman spectra shown in panel (c) [29]. The • symbols are experimental data obtained from [33], each data point being obtained using a different value of excitation laser energy. The ⋆ and ■ symbols are experimental data obtained for intravalley and intervalley double-resonance Raman processes in monolayer graphene, respectively [31]. The O,×, ⊕ and ∇ symbols are experimental data obtained from [27, 34, 35, 36]. (b) Eigenvectors for the phonons at the high-symmetry Γ and K (K′) points of the Brillouin zone. Each of these 12 modes is labeled and their atom displacements are indicated. i/o stands for in-plane/out-of-plane; T/L stands for transversal/longitudinal; A/O stands for acoustic/optical. The other symbols are symmetry assignments according to group theory [2, 6]. (c) Raman spectra from twisted bilayer graphene (tBLG) [29]. The peaks marked with * are activated by the superstructure modulation. The peaks at 303 cm^{-1} and 512 cm^{-1} come from the Si substrate where the sample is sitting. The peak at 1584 cm^{-1} is the G band.

range [16, 24, 25, 26, 27, 28, 29]. The filled symbols in the phonon dispersion plotted in Fig. 5.2(a) come from the so-called double-resonance Raman scattering effect [24, 30], where $q \neq 0$ phonons that generate resonant electron scattering between different points in the K and K′ valleys can be probed [31]. Changing the excitation laser energy changes the double-resonance selected q, and different places in the phonon Brillouin zone can be probed [24]. Another interesting effect is the stacking of two graphene layers with a mismatch rotation angle θ between the lattice structures in each layer,

building the so-called twisted bilayer graphene (tBLG) [16, 27, 28, 29]. The mismatch angle θ generates a superstructure where a potential modulation activates phonons with the modulation wavevector $q(\theta)$ [16, 27, 29, 32]. Figure 5.2(c) shows the Raman spectra from several tBLGs with different mismatch angles θ [29]. The peaks marked with * are Raman activated peaks from the interior of the Brillouin zone, and their frequencies are plotted in Fig. 5.2(a) with ◊ and □ symbols, allowing the use of Raman spectroscopy to measure the phonon dispersion in graphene.

In the phonon dispersion of graphene shown in Fig. 5.2(a), notice the appearance of a new branch (dashed line) labeled iTO′, fitting the □ and ● data. This branch is related to an interlayer vibration present only in many-layers graphene. N-layers graphene (N = number of layers) has $2N$ atoms in the unit cell, and they will be discussed in Section 5.2.

5.1.2 Graphene under Strain

Small modifications in the graphene structure may lead to different symmetry groups, sometimes related to other 2D materials [3]. For example, the structure of monolayer black or blue phosphorus (phosphorene) [37], silicone, and germanene [38] can be achieved by a distortion of the graphene lattice. Figure 5.1(a) shows that starting from the D_{6h}^{1} graphene a uniaxial compression induces a phase transition to subgroup D_{2h}^{11} of strained graphene. The hexagonal symmetry is lost, and the resulting structure is orthorhombic with all atoms in the same plane. Such a strain breaks the hexagonal symmetry, and two G bands are observed in the Raman spectra [8]. In order to accommodate such strain in the orthorhombic lattice, a possible distortion is to displace lines of atoms perpendicular to the plane periodically up and down [3]. These zig-zag lines of atoms displaced periodically perpendicular to the plane generate the structure of black P, which belongs to the D_{2h}^{7} subgroup. Otherwise, starting from the D_{6h}^{1} graphene symmetry (Fig. 5.1(b)) and applying an isotropic strain, changes are expected in the C—C bond distances, and such changes can be measured through changes in the G band frequency [6]. Relatively small homogeneous strain does not affect the symmetry of the system. For higher pressures, in order to accommodate the anisotropic strain, one possible distortion is to displace the atoms periodically up and down, perpendicularly to the plane, generating a trigonal arrangement of atoms. Such a distortion generates the structure of blue P (also of silicene, germanene, and stanene), which belongs to the D_{3d}^{3} subgroup [3]. Group theory has been used to gain insights into the symmetry aspects of graphene, black P, blue P, silicene, germanene, and stanene [3]. This analysis can be used to distinguish the different systems, and for a fast characterization of in-plane heterostructures that can be built to customize certain desired properties in these new materials.

5.2 Many-Layers Graphene and the Interlayer Vibrations in 2D Systems

5.2.1 In-Layer Vibrations

The symmetries for N-layer graphene, with N even or odd (from now on, $N \neq 1$), are the same as for bilayer and trilayer graphene, respectively [1, 2, 3]. The main symmetry

operation distinguishing the point groups between even and odd layers are the horizontal mirror plane, which is absent for N even, and the inversion, which is absent for N odd. At the Γ point, the point group is D_{3d} for N even and D_{3h} for N odd [2]. The consequences on the vibrational modes are mostly related to the fact that N-layers graphene has $2N$ atoms in the unit cell, thus multiplying the number of phonon branches. This aspect is behind the broad use of Raman spectroscopy as the main method when assigning the number of layers is a graphene sample [1, 5, 7, 39, 40]. Although the interlayer interactions are weak and no major change happens to the first-order phonon spectra, the changes in the second-order spectra subjected to the double-resonance condition is considerable, and generates the well-known method for N-assignment [6, 39, 40].

Graphite belongs to the $P6_3/mmc$ (D_{6h}^{4}) non-symorphic space group with only four atoms in the unit cell [2, 41]. The wavevector point groups are isomorphic to the wavevector point groups of monolayer graphene, but differ fundamentally for some classes where a translation of $c/2$ is present $\vec{c}$ is the unit cell vector normal to $\vec{a_1}$ and $\vec{a_2}$.

5.2.2 Interlayer Vibrations

Up to now, mostly vibrations within the two-dimensional planes have been discussed. These vibrations are usually characterized by relatively large phonon frequencies, and the stacking of multiple layers is of minor importance. There is another set of vibrations that are related to the coupling of two or more layers, which are the interlayer vibrations. The frequencies of the interlayer vibrations are much lower because the interlayer coupling in two-dimensional materials are governed by van der Walls bonds, which are much weaker than the in-plane covalent bonds [42, 43]. The physics of interlayer vibrations is independent on the specific in-plane symmetry, being general for two-dimensional materials with two layers or more, and can be used to monitor the number of layers and to study the evolution from the two-dimensional system to the bulk form.

There are two main types of interlayer vibrations: the shear (in-plane) and the breathing (out-of-plane) between two adjacent layers [44, 45, 46, 47, 48, 49, 50, 51, 52, 53, 54, 55, 56, 57, 58, 59, 60]. Figure 5.3(a) shows both types of vibrations for N = 2, 3, and 4. The number of different modes increases with $(N - 1)$.

In bilayer graphene, the shear mode vibrates at 28 cm^{-1}, while the interlayer breathing-mode frequency is close to 80 cm^{-1} [44, 47, 48, 49, 50, 51, 52]. Different works have reported the observation of shear modes from bilayer to bulk graphite using optical techniques such as Raman spectroscopy and coherent phonon spectroscopy [47, 48]. Figure 5.3(b) shows the measured differential reflectivity as a function of time for graphene samples with different numbers of layers. This experiment was accomplished using coherent phonon spectroscopy, where two pulsed laser beams (one pump, the other probe) were used, and the time delay between them could be tuned [48, 53]. The excitation generated by the pump pulses perturbs the interlayer potential in the few-layer graphene samples, launching the shear-mode oscillations. Since the duration of the pump pulse is shorter than the shear-mode period, the shear mode can be excited coherently. These coherent oscillations modulate the optical dielectric function of the

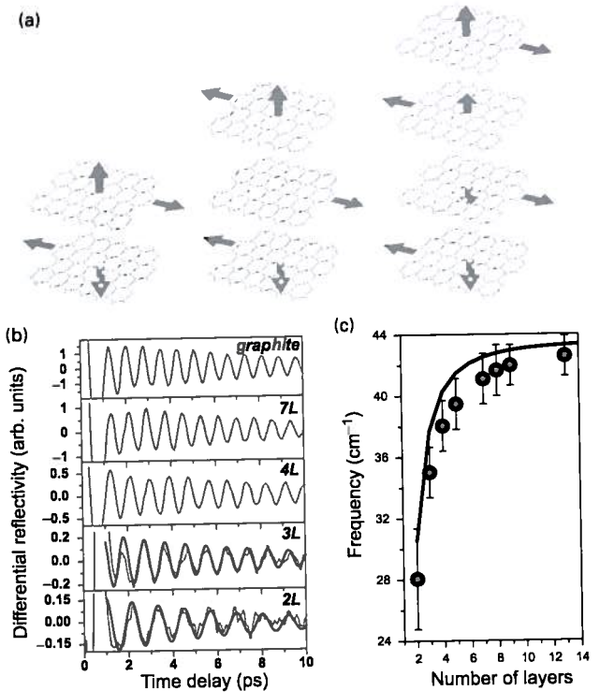

Fig. 5.3 (a) The shear vibrations, shown by the horizontal arrows, and the out-of-plane interlayer vibrations, shown by the vertical arrows, for graphene with number of layers $N = 2$, 3, and 4. (b) Differential reflectivity as a function of time for graphene samples with different number of layers, from two (2L) up to "infinite" (graphite) layers. The oscillations are due to the shear vibrations. (c) Dependence of the shear-mode frequency on the number of layers in multi-layer graphene samples. The symbols are experimental data and the line is a fit to the data using Eq. (5.1), with $\omega_\infty = 44$ cm^{-1} [48].

graphene layers, the amplitude of the modulation being proportional to the amplitude of the vibration [48, 53]. The Fourier transform of the experimental differential reflectivity data shown in Fig. 5.3(b) provides a measure of the shear-mode frequency as a function of the number of layers, as shown in Fig. 5.3(c). As shown in the graphics, the shear-mode frequency increases monotonically with the sample thickness [47, 48]. The shear and out-of-plane modes in few-layer graphene (as well as for other two-dimensional systems) are theoretically described by considering a coupled oscillator model, in which only interactions between identical adjacent layers are considered. The branch with the higher frequency corresponds to the shear motion of adjacent layers vibrating in opposite directions. The frequency of this branch for N-layers is given by

$$\omega_N = \omega_\infty \cos(\pi/2N), \tag{5.1}$$

where ω_∞ is the shear-mode frequency in the bulk limit [47, 48]. This model describes the trend of the experimental data (solid line in Fig. 5.3(c)), and the asymptotic behavior

predicts the shear-mode frequency of bilayer graphene to be lower than for bulk graphite by a factor $\sqrt{2}$.

Although we have focused our attention on the graphene case, the interlayer vibrations occur for all different classes of two-dimensional materials [47, 51, 54, 55, 56, 57, 58, 59, 60]. These vibrations provide a signature for the thicknesses of these two-dimensional systems, and open up new possibilities for studying interactions between adjacent layers or between the layers and the external environment (e.g. supporting substrate).

5.3 The Quantum Nature of Atomic Vibrations

Because of energy quantization, the low-energy acoustic phonon states are generally more populated than the high-energy optical phonon states. At a given temperature, the phonon population is described by the Bose–Einstein distribution function

$$n_0 = \frac{1}{e^{E_q/k_BT} - 1}, \tag{5.2}$$

where E_q and k_BT are the phonon and thermal energies, respectively [6, 61]. In the harmonic oscillator theory, the increase and decrease in the population number n is achieved by applying the creation ($a^\dagger$) and annihilation (a) operators, respectively, on an eigenstate $|n\rangle$. These operations introduce normalization factors given by $a^\dagger|n\rangle = (n+1)^{1/2}|n+1\rangle$ and $a|n\rangle = n^{1/2}|n-1\rangle$. Therefore, the phonon population can be measured in the inelastic scattering of light by phonons, where a photon creates or annihilates a phonon, in the so-called Stokes (S) or anti-Stokes (aS) Raman scattering processes, respectively (see Fig. 5.4(a)).

The intensity ratio between the Stokes and anti-Stokes signals (I_{aS}/I_S) is determined by the quantum mechanics normalization factors, i.e. $I_{aS}/I_S \propto n/(n+1)$ [6, 61]. Replacing n by the Bose–Einstein population function n_0 gives

$$\frac{I_{aS}}{I_S} = Ce^{E_q/k_BT}. \tag{5.3}$$

This equation can be inverted to obtain the effective phonon temperature in a material by measuring their Stokes and anti-Stokes–Raman spectra, given by

$$T = \frac{1}{k_B\left[\ln C - \ln\left(\frac{I_{aS}}{I_S}\right)\right]}, \tag{5.4}$$

where the constant C accounts for the optical properties of the system and can be found by setting T at room temperature for very low laser power (and zero bias in a graphene electronic device). This procedure has been largely used to study the phonon population dependence of different nanomaterial properties, such as electrical power [62], thermal conductivity [63], effective temperatures on biased nanostructures [64], phonon anharmonicities and lifetimes [65, 66], and optical transitions [67, 68].

However, Eq. (5.3) it is not universal. Special care should be taken when using Eq. (5.3) in materials with high-energy phonons like the G band in graphene. In this

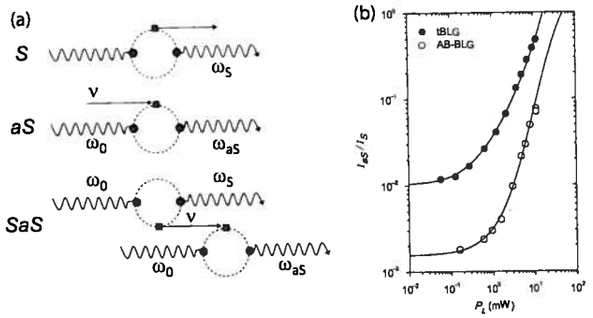

Fig. 5.4 (a) Feynman diagrams for the Stokes (*S*), anti-Stokes (*aS*) and Stokes–anti-Stokes (*SaS*) Raman scattering processes. Wavy and straight arrows stand for photons and phonons, respectively. Dashed circles represent electron–hole pairs, while black dots and black squares represent electron–photon and electron–phonon interactions, respectively. ω_0 and ν are the incident and the phonon fields frequencies, respectively, and $\omega_{S,aS}$ are the *S*, *aS* scattered field frequencies [70]. (b) Excitation laser power dependence for the I_{aS}/I_S intensity ratio from AB-stacked bi-layer graphene (open circles) and twisted-bilayer graphene (filled bullets) [70, 71]. The experimental data (symbols) were fit using Eq. (5.5) (see the text).

case, the thermally activated phonon population at room temperature is very low, and the anti-Stokes scattering may be dominated by a correlated phenomenon, called Stokes–anti-Stokes (*SaS*) scattering, where the same phonon is exchanged in the Stokes and the anti-Stokes scattering [see *SaS* in Fig. 5.4(a)] [69, 70]. To account for this phenomenon, Eq. (5.3) has to be generalized to include this effect, and the I_{aS}/I_S ratio is given by [71]

$$\frac{I_{aS}}{I_S} = C\frac{n_0}{n_0+1}[1 + C_{SaS}P_L], \tag{5.5}$$

where the term explicitly dependent on the excitation laser power (P_L) accounts for the *SaS* correlated scattering. The constant C_{SaS} measures the importance of the *SaS* phenomenon, and if C_{SaS} is negligibly small, Eq. (5.5) goes back to Eq. (5.3).

Evidence for the *SaS* process has been accumulating in materials science [70, 72, 73, 74, 75], generating interest in quantum optics [74, 75]. Since phonons have a significant lifetime (in the order of picoseconds [65, 66]), it has been proposed that these systems can work as a solid-state quantum memory, storing information between the write (*Stokes*) and read (*anti-Stokes*) processes [74]. For the optical phonons in graphene, the quantum memory would work at room temperature, because $E_q \gg k_BT$ at $T \sim 300$K. The correlated character of the Stokes and anti-Stokes photons can be continuously varied from purely quantum to purely classical, as demonstrated in diamond [75].

While many experiments have been performed in diamond with ultra-fast pulsed lasers to enhance the response of the non-linear *SaS* event, there is evidence for the observation of the dominant *SaS* event in graphene using a few miliwatts continuum wave (CW) laser, i.e. achievable even with a simple laser pointer. This result was obtained in a tBLG, specially engineered to exhibit resonance with the anti-Stokes photon emission [70]. In Fig. 5.4(b), the excitation power dependence of an AB-stacked bilayer graphene exhibits an I_{aS}/I_S power dependence that can be fit using Eq. (5.5) with $C_{SaS} = 0$ and an effective phonon temperature increasing linearly with the increasing excitation laser power. The excitation power dependence of the tBLG, however, clearly exhibits a linear dependence on P_L for larger excitation power values, and a fit using Eq. (5.5) shows that anti-Stokes photon production is dominated by the correlated *SaS* scattering [70, 71].

5.4 Phonon Coherence Length in Graphene

The phonon coherence length $\vec{c}$ is another important aspect of vibrations, playing an important role in the optical and transport properties of materials. For example, the high-energy optical phonons are known to limit electrical transport [62, 63, 64, 65]. Since phonons are studied in graphene mostly using light-scattering, the phonon coherence length will rule the length scale where spatial coherence takes place.

Spatial coherence defines the ability of two distinct points of a wave to interfere. The classic example of this phenomenon is the fringe visibility in a Young's double-slit interferometer. While broadly explored in optics, spatial coherence has been neglected in the light-scattering by phonons, because the field emitted by an incoherent source at a given wavelength λ is spatially uncorrelated on length-scales larger than $\lambda/2$ [76]. However, this approach is not valid if the non-radiating near-field components in the light–matter interaction are taken into account [77, 78, 79, 80]. It has been shown that, because of coherence, Raman intensities at the nanoscale depend significantly on the mode symmetry and spatial confinement of the vibration [81, 82].

In the case of graphene, it was theoretically predicted [81] and experimentally demonstrated [82] that the G band signal (E_{2g} symmetry) is subjected to destructive interference in the near-field regime. The results obtained from near-field Raman experiments revealed that these optical phonons in graphene are subject to coherence lengths $\vec{c} \approx 30$ nm [82].

For nanostructured materials whose average crystallite size L_a is smaller than the coherence length $\vec{c}$ of the phonons, the quantum confinement can generate frequency shift, broadening, and asymmetry of the peaks in the Raman spectra [6]. These changes are caused by the uncertainty in the phonon momentum associated with the finite size of crystallites. In other words, when $L_a < \vec{c}$, the Raman-allowed phonon wavevector q is relaxed by the amount $\Delta q \propto L_a^{-1}$. For this reason, the crystallite size L_a can be extracted from the width of the Raman lines in polycrystalline graphene systems with $L_a < \vec{c}$, as discussed in Section 5.5.

5.5 Probing Phonons Near Defects and Edges/Grain Boundaries

5.5.1 Disorder-Induced-Raman Processes in Graphene

Raman spectroscopy is considered as one of the most useful techniques for graphene characterization, with strong emphasis on defects [5, 6, 85, 86]. The key factor is the

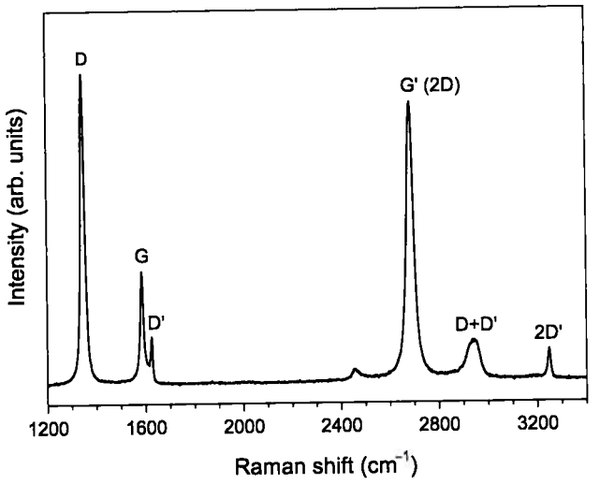

Fig. 5.5 Raman spectrum obtained from an ion-bombarded graphene sample with average distance between point defects $\vec{c} \approx 5$ nm [87].

occurrence of disorder-induced bands in the presence of defects, and their evolution with the amount and type of disorder. Figure 5.5 shows a Raman spectrum obtained from an ion-bombarded graphene sample [87]. This spectrum shows the first-order allowed G band (~1584 cm^{-1}), the second-order (or two-phonon) G′ (~2700 cm^{-1}, also called 2D band in the literature), and 2D′ (~3120 cm^{-1}) bands. The spectrum also shows three other additional disorder-induced bands, namely: the D band (~1350 cm^{-1}), the D′ band (~1620 cm^{-1}), and the combination D+D′ (~2970 cm^{-1}). Some important aspects and definitions about these features are:

- The D band originates from a totally symmetric vibration mode occurring near the corners (K or K′ points) of the first Brillouin zone (see eigenvector iTO at K in Fig. 5.1(b)) [88]. This mode belongs to the iTO phonon branch [89], and its Raman activity is mediated by a double-resonance mechanism in which the photoexcited electron or hole is scattered by a phonon (with finite wavevector $q_D \neq 0$), and back-scattered by a defect that provides momentum conservation in the process [30]. Because the phonon scatters an electron/hole from one Dirac cone to another, this process is called intervalley [24].
- The mechanism giving rise to the D′ band is similar to the one originating the D band (double resonance). The differences are: (i) the associated vibration mode belongs to the iLO phonon branch, occurring near the center of the first-Brillouin zone, although the phonon wavevector is still finite, i.e. $q_{D'} \neq 0$; (ii) since the phonon wavevector is much shorter than the one giving rise to the D band, the electron is scattered by the phonon from one eigenstate to another belonging to the same Dirac cone. For this reason, this process is called intravalley [5, 6, 7, 24, 30].

- The G′ (2D) and 2D′ bands originate from the overtone of the phonon modes that give rise to the D and D′ bands, respectively [5, 6, 7, 24, 30, 90]. Since the electron (or hole) is scattered twice by the same phonon (with opposite wavevectors), the G′ and 2D′ do not require the defects to be observed.
- Unlike the G′ and 2D′ bands, the combination D+D′ requires the presence of defects for momentum conservation, since the D and D′ phonon wavevectors have different magnitudes ($|q_D| \neq |q_{D'}|$) in the scattering process [91].

5.5.2 Types of Defects and Their Influence on the Disorder-Induced Bands

Long-Range versus Short-Range Defects

Because the magnitude of the wavevector of the phonon giving rise to the D band is relatively large (if compared to the total extension of the first Brillouin zone), the D band is only activated by short-range defects [15]. In other words, the defect has to be confined to a small region in the real-space in order to provide such a large momentum in the reciprocal space. Structural defects such as vacancies, edges, and crystallite borders belong to this class of short-range defects, and therefore the D band is activated. On the other hand, the wavevector of the phonon associated with the D′ band is considerably shorter, and therefore the D′ band can be activated by long-range defects such as charged impurities absorbed on the graphene sheet [15]. For these reasons, the ratio between the D and D′ intensities can be used to probe the nature of the defects, being larger for long-range defects than for short-range ones [92].

Edges/Grain Boundaries

Regarding graphene edges, and considering that the grain boundary is a type of graphene edge, two important points are highlighted.

- Both D and D′ intensities are strongly dependent on the direction of the polarization vector $\boldsymbol{P}$ of the exciting field relative to the edge direction, following the relation

$$I_{D,D'} \propto \cos^4 \alpha, \tag{5.6}$$

  where $I_{D,D'}$ is the intensity of the D, D′ scattered field, and α is the angle between $\boldsymbol{P}$ and the edge direction [93, 94]. Therefore, these two features present maximum intensities for incident light with the polarization field parallel to the edge, and minimum (null for perfect edges) for incident light with the polarization field perpendicular to the edge [94, 95].
- The D band exhibits maximum intensity for armchair edges, and cannot be activated by zig-zag edges. This property can be used to probe the crystallographic orientation of graphene edges [94, 95]. The atomic structure of the edges plays no role in the D′ scattering.

5.5.3 Quantifying the Amount of Disorder by Raman Spectroscopy

The ratio between the D and G band integrated intensities (I_D/I_G) has been broadly used to measure the amount of disorder in nanostructured graphitic samples [4, 5, 6, 7]. Care should be taken when reading the literature because some authors use the intensity (peak height) ratio and others use the integrated intensity (peak area) ratio. The first approach was originally introduced by Tuinstra and Koenig [88]. By noticing that the D band is activated by the borders of crystallites in nanographitic samples, the authors proposed that its intensity should be scaled with the perimeter of the crystallites, that is, $I_D \propto L_a$, with L_a being the lateral dimension of the crystallite. On the other hand, the G band intensity should be proportional to the crystallite area ($I_G \propto {L_a}^2$). Based on these two geometrical assumptions, Tuinstra and Koenig proposed the proportionality relation $I_D/I_G \propto 1/L_a$. Later on, Ferrari and Robertson noticed that the relation proposed by Tuinstra and Koenig was no longer valid for samples with a high-degree of disorder, for which they proposed the relation $I_D/I_G \propto {L_a}^2$ [89].

Both relations (Tuinstra and Koenig ($I_D/I_G \propto 1/L_a$), and Ferrari and Robertson ($I_D/I_G \propto {L_a}^2$)) are based in a single parameter, which is the crystallite size L_a. In order to introduce a unified approach, Lucchese and collaborators [87] proposed a phenomenological model to explain the evolution of the I_D/I_G ratio in a graphene sheet with points defects, as a function of the average distance L_D among defects. In this model, two new parameters are introduced: (i) the radius (r_S) of the structurally disordered area, which is a measure of the defect size; and (ii) the radius (r_A) of the area where the D band scattering takes place, $r_A > r_S$. While r_S is defined as a purely structural parameter, r_A is a dynamical variable related to the coherence length of the photoexcited electrons or holes involved in the D band scattering.

A similar model was applied for polycrystalline graphene samples with average crystallite size L_a [84]. In this case, the length of the D band activation area (L_A) near the borders of the crystallites replaces r_A, and the thickness L_S of the structurally disordered area surrounding the crystallite ($L_S \approx L_B/2$, where L_B is the thickness of the grain boundary between two merged crystallites) replaces r_S. The two models have the same geometrical reasoning, but in one case the defects are point-like (zero-dimensional, 0D) and in the other the defects are line-like (one-dimensional, 1D). The experimental values obtained for these parameters were $r_A \approx L_A \approx 4$ nm [84, 87], $r_S \approx 1$ nm [87], and $L_S \approx 2$ nm [84].

The I_D/I_G ratio depends on the wavelength of the excitation laser source, λ_L [96, 97, 98]. While the G band intensity is proportional to ${\lambda_L}^{-4}$ (as usual for first-order Raman scattering processes [6]), the D band intensity does not depend considerably on λ_L [96], and therefore the general trend $I_D/I_G \propto {\lambda_L}^4$ was experimentally observed for λ_L, within the visible range [84, 91, 96, 98].

Figures 5.6(a) and (b) show the plots of the relations obtained for the I_D/I_G ratio as a function of L_D (Fig. 5.6(a)) and L_a (Fig. 5.6(b)), considering different excitation laser wavelengths. These plots summarize the results presented in [87, 91] and [84], and can be used as a guide to estimate L_D and L_a, respectively.

For samples with point defects separated by $L_D \geq 10$ nm, the experimental results presented in [87, 91] lead to

$$L_D^2\ (\text{nm}) = \left(1.8 \times 10^{-9}\right)\lambda_L^4 (I_D/I_G)^{-1}. \tag{5.7}$$

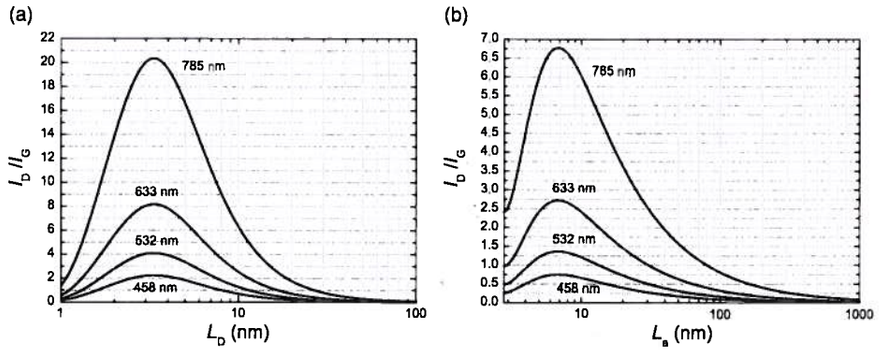

Fig. 5.6 Plots of the relations obtained for the I_D/I_G ratio as a function of L_D (0D defects, panel (a)) [87, 91] and L_a (1D defects, panel (b)) [84], considering four different excitation laser wavelengths (as indicated in the graphics).

For $L_D < 10$ nm, I_D/I_G deviates from this simple equation [87] and the broadening effects take place [99].

In the case of the nanostructured graphene with the crystallite sizes larger than the phonon coherence length, i.e. $L_a \geq 30$ nm (see Section 5.4), the Tuinstra and Koenig proportionality relation holds, and the experimental results yield [84, 98]

$$L_a\ (\text{nm}) = \left(2.4 \times 10^{-10}\right)\lambda_L^4 (I_D/I_G)^{-1}. \tag{5.8}$$

For $L_a < 30$ nm, the I_D/I_G deviates from this simple equation [84], and the G band broadening provides a more accurate figure of merit, obeying the relation [84]

$$\Gamma_G(L_a) = 15 + 95e^{-2L_a/30}. \tag{5.9}$$

Equations 5.7–5.8 and Fig. 5.6 can be used for quantifying defects/disorder in graphene systems. For the dependence on the number of layers, see [99, 100].

5.6 References

[1] M. S. Dresselhaus, G. Dresselhaus, and A. Jorio, *Group Theory: Application to the Physics of Condensed Matter* (Springer-Verlag, 2008).

[2] L. M. Malard, M. H. D. Guimarães, D. L. Mafra, M. S. C. Mazzoni, and A. Jorio, Group-theory analysis of electrons and phonons in *N*-layer graphene systems. *Physical Review B*, **79** (2009), 125426.

[3] J. Ribeiro-Soares, R. M. Almeida, L. G. Cançado, M. S. Dresselhaus, and A. Jorio, Group theory for structural analysis and lattice vibrations in phosphorene systems. *Physical Review B*, **91** (2015), 205421.

[4] S. Reich and C. Thomsen, Raman spectroscopy of graphite. *Philosophical Transactions of the Royal Society of London. Series A: Mathematical, Physical and Engineering Sciences*, **362**:1824 (2004), 2271–88.

[5] A. C. Ferrari, Raman spectroscopy of graphene and graphite: Disorder, electron–phonon coupling, doping and nonadiabatic effects. *Solid State Communications*, **143**:1 (2007), 47–57.

[6] A. Jorio, M. S. Dresselhaus, and R. Saito, *Raman Spectroscopy in Graphene Related Systems* (Wiley-VCH, 2011).
[7] A. C. Ferrari and D. M. Basko, Raman spectroscopy as a versatile tool for studying the properties of graphene. *Nature Nanotechnology*, **8** (2013), 235–46.
[8] M. Huang, H. Yan, C. Chen, D. Song, T. F. Heinz, and J. Hone, Phonon softening and crystallographic orientation of strained graphene studied by Raman spectroscopy. *Proceedings of the National Academy of Sciences*, **106**:18 (2009), 7304–8.
[9] A. Das, S. Pisana, B. Chakraborty, S. Piscanec, S. K. Saha, U.V. Waghmare, K. S. Novoselov, H. R. Krishnamurthy, A. K. Geim, A. C. Ferrari, and A. K. Sood, Monitoring dopants by Raman scattering in an electrochemically top-gated graphene transistor. *Nature Nanotechnology*, **3**:4 (2008), 210–15.
[10] A. A. Balandin, S. Ghosh, W. Bao, I. Calizo, D. Teweldebrhan, F. Miao, and C. Ning Lau, Superior thermal conductivity of single-layer graphene. *Nano Letters*, **8**:3(2008), 902–7.
[11] M. Acik, G. Lee, C. Mattevi, M. Chhowalla, K. Cho, and Y. J. Chabal, Unusual infrared-absorption mechanism in thermally reduced graphene oxide. *Nature Materials*, **9**(2010), 840–5.
[12] G. Dovbeshko, O. Gnatyuk, O. Fesenko, A. Rynder, and O. Posudievsky, Enhancement of infrared absorption of biomolecules absorbed on single-wall carbon nanotubes and graphene nanosheets. *Journal of Nanophotonics*, **6**:1 (2012), 061711.
[13] L. M. Zhang, Z. Q. Li, D. N. Basov, M. M. Fogler, Z. Hao, and M. C. Martin, Determination of the electronic structure of bilayer graphene from infrared spectroscopy. *Physical Review B*, **78**:23 (2008), 235408.
[14] Z. Q. Li, E. A. Henriksen, Z. Jiang, Z. Hao, M. C. Martin, P. Kim, and D. N. Basov, Dirac charge dynamics in graphene by infrared spectroscopy. *Nature Physics*, **4**:7 (2008), 532–5.
[15] P.Venezuela, M. Lazzeri, and F. Mauri, Theory of double-resonant Raman spectra in graphen: Intensity and line shape of defect-induced and two-phonon bands. *Physical Review B*, **84** (2011), 035433.
[16] A. Jorio and L. G. Cançado. Raman spectroscopy of twisted bilayer graphene. *Solid State Communications*, **175–6** (2013), 3–12
[17] L. Wirtz and A. Rubio, The phonon dispersion of graphite revisited. *Solid State Communications*, **131**:3 (2004), 141–52.
[18] O. Dubay, G. Kresse, and H. Kuzmany, Phonon softening in metallic nanotubes by a Peierls-like mechanism. *Physical Review Letters*, **88**(2002), 235506.
[19] S. Piscanec, M. Lazzeri, F. Mauri, A. C. Ferrari, and J. Robertson, Kohn anomalies and electron–phonon interactions in graphite. *Physical Review Letters*, **93**:18 (2004), 185503.
[20] S. Pisana, M. Lazzeri, C. Casiraghi, K. S. Novoselov, A. K. Geim, A. C. Ferrari, and F. Mauri, Breakdown of the adiabatic Born–Oppenheimer approximation in graphene. *Nature Materials*, **6**:3 (2007), 198–201.
[21] M. Lazzeri, C. Attaccalite, L. Wirtz, and F. Mauri, Impact of the electron–electron correlation on phonon dispersion: Failure of LDA and GGA DFT functionals in graphene and graphite. *Physical Review B*, **78**:8 (2008), 081406.
[22] M. Mohr, J. Maultzsch, E. Dobardžić, S. Reich, I. Milošević, M. Damnjanović, A. Bosak, M. Krisch, and C. Thomsen, Phonon dispersion of graphite by inelastic X-ray scattering. *Physical Review B*, **76**:3 (2007), 035439.
[23] A. Grüneis, J. Serrano, A. Bosak, M. Lazzeri, S. L. Molodtsov, L. Wirtz, and T. Pichler, Phonon surface mapping of graphite: Disentangling quasi-degenerate phonon dispersions. *Physical Review B*, **80**:8 (2009), 085423.

[24] R. Saito, A. Jorio, A. G. Souza Filho, G. Dresselhaus, M. S. Dresselhaus, and M. A. Pimenta, Probing phonon dispersion relations of graphite by double resonance Raman scattering. *Physical Review Letters*, **88** (2001), 027401.
[25] D. L. Mafra, G. Samsonidze, L. M. Malard, D. C. Elias, J. C. Brant, F. Plentz, E. S. Alves, and M. A. Pimenta, Determination of LA and TO phonon dispersion relations of graphene near the Dirac point by double resonance Raman scattering. *Physical Review B*, **76**:23 (2007), 233407.
[26] O. Frank, M. Mohr, J. Maultzsch, C. Thomsen, I. Riaz, R. Jalil, and C. Galiotis, Raman 2D-band splitting in graphene: theory and experiment. *ACS Nano*, **5**:3 (2011), 2231–9.
[27] V. Carozo, C. M. Almeida, E. H. M. Ferreira, L. G. Cançado, C. A. Achete, and A. Jorio, Raman signature of graphene superlattices. *Nano Letters*, **11**:11 (2011), 4527–34.
[28] A. Righi, S. D. Costa, H. Chacham, C. Fantini, P. Venezuela, C. Magnuson, L. Colombo, W. S. Bacsa, R. S. Ruoff, and M. A. Pimenta, Graphene moiré patterns observed by Umklapp double-resonance Raman scattering. *Physical Review B*, **84**:24(2011), 241409.
[29] J. Campos-Delgado, L. G. Cançado, C. A. Achete, A. Jorio, and J.-P. Raskin, Raman scattering study of the phonon dispersion in twisted bilayer graphene. *Nano Research*, **6**:4 (2013), 269–74.
[30] C. Thomsen and S. Reich, Double resonant Raman scattering in graphite. *Physical Review Letters*, **85** (2000), 5214.
[31] S. Bernard, E. Whiteway, V. Yu, D. G. Austing, and M. Hilke, Probing the experimental phonon dispersion of graphene using ^{12}C and ^{13}C isotopes. *Physical Review B*, **86** (2012), 085409.
[32] V. Carozo, C. M. Almeida, B. Fragneaud, P. Bedê, J. Moutinho, M. V. O. Ribeiro-Soares, N. Andrade, A. G. Souza Filho, M. J. S. Matos, B. Wang, M. Terrones, R. B. Capaz, A. Jorio, C. A. Achete, and L. G. Cançado, Resonance effects on the Raman spectra of graphene superlattices. *Physical Review B*, **88** (2013), 085401.
[33] C. H. Lui, L. M. Malard, S. H. Kim, G. Lantz, F. E. Leverge, R. Saito, and T. Heinz, Observation of layer-breathing mode vibrations in few-layer graphene through combination Raman scattering. *Nano Letters*, **12**:11 (2012), 5539–44.
[34] K. Kim, S. Coh, L. Z. Tan, W. Regan, J. M. Yuk, E. Chatterjee, M. F. Crommie, M. L. Cohen, S. G.Louie, and A. Zettl, Raman spectroscopy study of ratated double-layer graphene: misorientation-angle dependence of electronic structure. *Physical Review Letters*, **108** (2012), 246103.
[35] R. W. Havener, H. Zhuang, L. Brown, R. G. Hennig, and J. Park, Angle-resolved Raman imaging of interlayer rotations and interactions in twisted bilayer graphene. *Nano Letters*, **12**:6 (2012), 3162–7.
[36] Y. Wang, Z. Su, W. Wu, S. Nie, N. Xie, H. Gong, Y. Guo, J. H. Lee, X. Xing, S. Lu, H. Wang, X. Lu, K. McCarty, F. Pei, S. Robles-Hernandez, V. G. Hadjiev, and J. Bao, Twisted bilayer graphene superlattices, arXiv:1301.4488v1.
[37] P. Li and I. Appelbaum, Electrons and holes in phosphorene. *Physical Review B*, **90** (2014), 115439.
[38] K. Takeda and K. Shiraishi, Theoretical possibility of stage corrugation in Si and Ge analogs of graphite. *Physical Review B*, **50** (1994), 14916.
[39] A. C. Ferrari, J. C. Meyer, V. Scardaci, C. Casiraghi, M. Lazzeri, F. Mauri, S. Piscanec, D. Jiang, K. S. Novoselov, S. Roth, and A. K. Geim, Raman spectrum of graphene and graphene layers. *Physical Review Letters*, **97** (2006), 187401.
[40] L. M. Malard, M. A. Pimenta, G. Dresselhaus, and M. S. Dresselhaus, Raman spectroscopy in graphene. *Physics Reports*, **473**:5–6 (2009), 51–88.

[41] L. G. Cançado, A. Reina, J. Kong, and M. S. Dresselhaus, Geometrical approach for the study of G′ band in the Raman spectrum of monolayer graphene, bilayer graphene, and bulk graphite. *Physical Review B*, **77** (2008), 245408.

[42] R. Nicklow, N. Wakabayashi, and H. G. Smith, Lattice dynamics of pyrolytic graphite. *Physical Review B*, **5** (1972), 4951–62.

[43] M. T. Yin and M. L. Cohen, Structural theory of graphite and graphitic silicon. *Physical Review B*, **29** (1984), 6996.

[44] Jin-Wu Jiang, Hui Tang, Bing-Shen Wang, and Zhao-Bin Su, Raman and infrared properties and layer dependence of the phonon dispersions in multilayered graphene. *Physical Review B*, **77** (2008), 235421.

[45] K. H. Michel and B. Verberck, Theory of rigid-plane phonon modes in layered crystals. *Physical Review B*, **85** (2012), 094303.

[46] V. N. Popov and C. Van Alsenoy, Low-frequency phonons of few-layer graphene within a tight-binding model. *Physical Review B*, **90** (2014), 245429.

[47] P. H. Tan, W. P. Han, W. J. Zhao, Z. H. Wu, K. Chang, H. Wang, Y. F. Wang, N. Bonini, N. Marzari, N. Pugno, G. Savini, A. Lombardo, and A. C. Ferrari, The shear mode of multilayer graphene. *Nature Materials*, **11** (2012), 294–300.

[48] D. Boschetto, L. Malard, C. H. Lui, K. F. Mak, Z. Li, H. Yan, and T. F. Heinz, Real-time observation of interlayer vibrations in bilayer and few-layer graphene. *Nano Letters*, **13** (2013), 4620–3.

[49] C. H. Lui, L. M. Malard, S. Kim, G. Lantz, F. E. Laverge, R. Saito, and T. F. Heinz, Observation of layer-breathing mode vibrations in few-layer graphene through combination Raman scattering. *Nano Letters*, **12** (2012), 5539–44.

[50] C. H. Lui and T. F. Heinz, Measurement of layer breathing mode vibrations in few-layer graphene. *Physical Review B*, **87** (2013), 121404(R).

[51] Chunxiao Cong and Ting Yu, Enhanced ultra-low-frequency interlayer shear modes in folded graphene layers. *Nature Communications*, **5** (2014), 4709.

[52] C. H. Lui, Z. Ye, C. Keiser, X. Xiao, and R. He, Temperature-activated layer-breathing vibrations in few-layer graphene. *Nano Letters*, **14** (2014), 4615–21.

[53] T. Mishina, K. Nitta, and K. Y. Masumoto, Coherent lattice vibration of interlayer shearing mode of graphite. *Physical Review B*, **62** (2000), 2908.

[54] X. Zhang, W. P. Han, J. B. Wu, S. Milana, Y. Lu, Q. Q. Li, A. C. Ferrari, and P. H. Tan, Raman spectroscopy of shear and layer breathing modes in multilayer MoS_2. *Physical Review B*, **87** (2013), 115413.

[55] X. Zhang, X. F. Qiao, W. Shi, J.B. Wu, D. S. Jiang, and P. H. Tan, Phonon and Raman scattering of two-dimensional transition metal dichalcogenides from monolayer, multilayer to bulk material. *Chemical Society Review*, **44** (2015), 2757–85.

[56] Y. Zhao, X. Luo, H. Li, J. Zhang, P. T. Araujo, C. K. Gan, J. Wu, H. Zhang, S. Y. Quek, M. S. Dresselhaus, and Q. Xiong, Interlayer breathing and shear modes in few-trilayer MoS_2 and WSe_2. *Nano Letters*, **13** (2013), 1007–15.

[57] K. Liu, L. Zhang, T. Cao, C. Jin, D. Qiu, Q. Zhou, A. Zettl, P. Yang, S. G. Louie, and F. Wang, Evolution of interlayer coupling in twisted molybdenum disulfide bilayers. *Nature Communications*, **5** (2014), 4966.

[58] C. H. Lui, Z. Ye, C. Ji, K. C. Chiu, C. T. Chou, T. I. Andersen, C. Means-Shively, H. Anderson, J. M. Wu, T. Kidd, Y. H. Lee, and R. He, Observation of interlayer phonon modes in van der Waals heterostructures. *Physical Review B*, **91** (2015), 165403.

[59] S. Ge, X. Liu, X. Qiao, Q. Wang, Z. Xu, J. Qiu, P. H. Tan, J. Zhao, and D. Sun, Coherent longitudinal acoustic phonon approaching THz frequency in multilayer molybdenum disulphide. *Scientific Reports*, **4** (2014), 5722.

[60] Jiang-Bin Wu, Zhi-Xin Hu, X. Zhang, Wen-Peng Han, Y. Lu, W. Shi, Xiao-Fen Qiao, M. Ijiäs, S. Milana, W. Ji, A. C. Ferrari, and Ping-Heng Tan, Interface coupling in twisted multilayer graphene by resonant Raman spectroscopy of layer breathing modes. *ACS Nano*, **9** (2015), 7440–9.

[61] D. J. Gardiner, *Practical Raman Spectroscopy*. (Springer-Verlag, 1989).

[62] M. Steiner, M. Freitag, V. Perebeinos, J. C. Tsang, J. P. Small, M. Kinoshita, D. Yuan, J. Liu, and P. Avouris. Phonon populations and electrical power dissipation in carbon nanotube transistors. *Nature Nanotechnology*, **4** (2009), 320.

[63] C. Faugeras, B. Faugeras, M. Orlita, M. Potemski, R. R. Nair, and A. K. Geim, Thermal conductivity of graphene in corbino membrane geometry. *ACS Nano*, **4** (2010), 1889.

[64] S. Berciaud, M. Y. Han, K. F. Mak, L. E. Brus, P. Kim, and T. F. Heinz, Electron and optical phonon temperatures in electrically biased graphene. *Physical Review Letters*, **104** (2010), 227401.

[65] N. Bonini, M. Lazzeri, N. Marzari, and F. Mauri, Phonon anharmonicities in graphite and graphene. *Physical Review Letters*, **99** (2007), 176802.

[66] D. Song, F. Wang, G. Dukovic, M. Zheng, E. D. Semke, L. E. Brus, and T. F. Heinz, Direct measurement of the lifetime of optical phonons in single-walled carbon nanotubes. *Physical Review Letters*, **100** (2008), 225503.

[67] A. Jorio, A. G. Souza Filho, G. Dresselhaus, M. S. Dresselhaus, R. Saito, J. H. Hafner, C. M. Lieber, F. M. Matinaga, M. S. S. Dantas, and M. A. Pimenta, Joint density of electronic states for one isolated single-wall carbon nanotube studied by resonant Raman scattering. *Physical Review B*, **63** (2001), 245416.

[68] A. G. Souza Filho, A. Jorio, J. H. Hafner, C. M. Lieber, R. Saito, M. A. Pimenta, G. Dresselhaus, and M. S. Dresselhaus, Electronic transition energy E_{ii} for an isolated (n, m) single-wall carbon nanotube obtained by anti-Stokes/Stokes resonant Raman intensity ratio. *Physical Review B*, **63** (2001), 241404(R).

[69] D. N. Klyshko, Correlation between the Stokes and anti-Stokes components in inelastic scattering of light. *Soviet Journal of Quantum Electronics*, **7** (1977), 755.

[70] A. Jorio, M. Kasperczyk, N. Clark, E. Neu, P. Maletinsky, A. Vijayaraghavan, and L. Novotny, Optical-phonon resonances with saddle-point excitons in twisted-bilayer graphene. *Nano Letters*, **14** (2014), 5687.

[71] C. A. Parra-Murillo, M. F. Santos, C. H. Monken, and A. Jorio, Stokes–anti-Stokes correlation in the inelastic scattering of light by matter and generalization of the Bose–Einstein population function. *Physical Review B*, **93** (2016), 125141.

[72] M. Kasperczyk, F. S. de Aguiar Júnior, C. Rabelo, A. Saraiva, M. F. Santos, L. Novotny, and A. Jorio. Temporal quantum correlations in inelastic light scattering from water. *Physical Review Letters*, **117** (2016), 243603.

[73] K. Kang, D. Abdula, D.G. Cahill, and M. Shim. Lifetimes of optical phonons in graphene and graphite by time-resolved incoherent anti-Stokes–Raman scattering. *Physical Review B*, **81** (2010), 165405.

[74] K. C. Lee, B. J. Sussman, M. R. Sprague, P. Michelberger, K. F. Reim, J. Nunn, N. K. Langford, P. J. Bustard, D. Jaksch, and I. A. Walmsley, Macroscopic non-classical states and terahertz quantum processing in room-temperature diamond. *Nature Photonics*, **6** (2012), 41.

[75] M. Kasperczyk, A. Jorio, E. Neu, P. Maletinksy, and L. Novotny, Stokes–anti-Stokes correlations in Raman scattering from diamond membranes. *Optics Letters*, **40** (2015), 2393.
[76] W. H. Carter and E. Wolf, Coherence properties of Lambertian and non-Lambertian sources. *Journal of the Optical Society of America*, **65** (1975), 1067.
[77] R. Carminati and J.-J. Greffet, Near-field effects in spatial coherence of thermal sources. *Physical Review Letters*, **82** (1999), 1660.
[78] A. V. Shchegrov, K. Joulain, R. Carminati, and J.-J. Greffet, Near-field spectral effects due to electromagnetic surface excitations. *Physical Review Letters*, **85** (2000), 1548.
[79] H. Roychowdhury and E. Wolf, Effects of spatial coherence on near-field spectra. *Optics Letters*, **28** (2003), 170.
[80] A. Apostol and A. Dogariu, Spatial correlations in the near field of random media. *Physical Review Letters*, **91** (2003), 093901.
[81] L. G. Cançado, R. Beams, A. Jorio, and L. Novotny, Theory of spatial coherence in near-field Raman scattering. *Physical Review X*, **4** (2014), 031054.
[82] R. Beams, L. G. Cançado, S.-H. Oh, A. Jorio, and L. Novotny, Spatial coherence in near-field Raman scattering. *Physical Review Letters*, **113** (2014), 186101.
[83] H. Richter, Z. P. Wang, and L. Ley, The one phonon Raman spectrum in microcrystalline silicon. *Solid State Communications*, **39** (1981), 625.
[84] J. Ribeiro-Soares, M. E. Oliveros, C. Garin, M. V. David, L. G. P. Martins, C. A. Almeida, E. H. Martins-Ferreira, K. Takai, T. Enoki, R. Magalhães-Paniagoa, A. Malachias, A. Jorio, B. S. Archanjo, C. A. Achete, and L. G. Cançado, Structural analysis of polycrystalline graphene systems by Raman spectroscopy. *Carbon*, **95** (2015), 646–52.
[85] R. Beams, L. G. Cançado, and L. Novotny, Raman characterization of defects and dopants in graphene. *Journal of Physics: Condensed Matter*, **27** (2015), 083002.
[86] M. A. Pimenta, G. Dresselhaus, M. S. Dresselhaus, L. G. Cançado, A. Jorio, and R. Saito, Studying disorder in graphite-based systems by Raman spectroscopy. *Physical Chemistry Chemical Physics*, **9** (2007), 1276.
[87] M. M. Lucchese, F. Stavale, E. H. Ferriera, C. Vilane, M. V. O. Moutinho, R. B. Capaz, C. A. Achete, and A. Jorio, Quantifying ion-induced defects and Raman relaxation length in graphene. *Carbon*, **48** (2010), 1592.
[88] F. Tuinstra and J. L. Koenig, Raman spectrum of graphite. *Journal of Chemical Physics*, **53** (1970), 1126.
[89] A. C. Ferrari and J. Robertson, Resonant Raman spectroscopy of disordered, amorphous, and diamondlike carbon. *Physical Review B*, **64** (2001), 075414.
[90] L. G. Cançado, M. A. Pimenta, R. Saito, A. Jorio, L. O. Ladeira, A. Grueneis, A. G. Souza-Filho, G. Dresselhaus, and M. S. Dresselhaus, Stokes and anti-Stokes double resonance Raman scattering in two-dimensional graphite, *Physical Review B*, **66** (2002), 035415.
[91] L. G. Cançado, A. Jorio, E. H. Martins Ferreira, F. Stavale, C. A. Achete, R. B. Capaz, M. V. O. Moutinho, A. Lombardo, T. S. Kulmala, and A. C. Ferrari, Quantifying defects in graphene via Raman spectroscopy at different excitation energies. *Nano Letters*, **11** (2011), 3190.
[92] A. Eckmann, A. Felten, A. Mishchenko, L. Britnell, R. Krupke, K. S. Novoselov, and C. Casiraghi, Probing the nature of defects in graphene by Raman spectroscopy. *Nano Letters*, **12** (2012), 3925.
[93] A. Grüneis, R. Saito, Ge. G. Samsonidze, T. Kimura, M. A. Pimenta, A. Jorio, A. G. Souza Filho, G. Dresselhaus, and M. S. Dresselhaus. Inhomogeneous optical absorption around the K point in graphite and carbon nanotubes. *Physical Review B*, **67** (2003), 165402.

[94] L. G. Cançado, M. A. Pimenta, B. R. A. Neves, M. S. Dantas, and A. Jorio, Influence of the atomic structure on the Raman spectra of graphite edges. *Physical Review Letters*, **93** (2004), 247401.
[95] C. Casiraghi, A. Hartschuh, H. Qian, S. Piscanec, C. Georgi, A. Fasoli, K. S. Novoselov, D. M. Basko, and A. C. Ferrari, Raman spectroscopy of graphene edges. *Nano Letters*, **9** (2009), 1433.
[96] L. G. Cançado, A. Jorio, and M. A. Pimenta, Measuring the absolute Raman cross section of nanographites as a function of laser energy and crystallite size. *Physical Review B*, **76** (2007), 064304.
[97] P. Klar, E. Lidorikis, A. Eckmann, I. A. Verzhbitskiy, A. C. Ferrari, and C. Casiraghi. Raman scattering efficiency of graphene, *Physical Review B*, **87** (2013), 205435.
[98] L. G. Cançado, K. Takai, T. Enoki, M. Endo, Y. A. Kim, H. Mizusaki, A. Jorio, L. N. Coelho, R. Magalhães-Paniago, and M. A. Pimenta, General equation for the determination of the crystallite size L[a] of nanographite by Raman spectroscopy. *Applied Physics Letters*, **88** (2006), 163106.
[99] E. H. Martins Ferreira, M. V. O. Moutinho, F. Stavale, M. M. Lucchese, R. B. Capaz, C. A. Achete, and A. Jorio, Evolution of the Raman spectra from single-, few-, and many-layer graphene with increasing disorder. *Physical Review B*, **82** (2010), 125429.
[100] R. Giro, B. S. Archanjo, E. H. Martins Ferreira, R. B. Capaz, A. Jorio, and C. A. Achete. Quantifying defects in N-layer graphene via a phenomenological model of Raman spectroscopy. *Nuclear Instruments and Methods in Physics Research Section B*, **319** (2014), 71–4.